DFT Analysis of the Reaction Paths of Formaldehyde Decomposition on Silver

Alejandro Montoya* and Brian S. Haynes

School of Chemical and Biomolecular Engineering, The University of Sydney, Sydney, NSW 2006, Australia

Received: February 7, 2009; Revised Manuscript Received: May 18, 2009

Periodic density functional theory is used to study the dehydrogenation of formaldehyde (CH_2O) on the Ag(111) surface and in the presence of adsorbed oxygen or hydroxyl species. Thermodynamic and kinetic parameters of elementary surface reactions have been determined. The dehydrogenation of CH_2O on clean Ag(111) is thermodynamically and kinetically unfavorable. In particular, the activation energy for the first C−H bond scission of adsorbed CH_2O (25.8 kcal mol^{-1}) greatly exceeds the desorption energy for molecular CH_2O (2.5 kcal mol^{-1}). Surface oxygen promotes the destruction of CH_2O through the formation of CH_2O_2, which readily decomposes to CHO_2 and then in turn to CO_2 and adsorbed hydrogen. Analysis of site selectivity shows that CH_2O_2, CHO_2, and CHO are strongly bound to the surface through the bridge sites, whereas CO and CO_2 are weakly adsorbed with no strong preference for a particular surface site. Dissociation of CO and CO_2 on the Ag(111) surface is highly activated and therefore unfavorable with respect to their molecular desorption.

Introduction

The kinetics and mechanism of CH_2O interaction with solid surfaces is of particular significance for modeling catalytic processes such as CO hydrogenation, methyl formate and alcohol synthesis, and dehydrogenation of CH_3OH and for controlling indoor pollutant in airtight buildings.[1] The kinetics of the thermal decomposition of CH_2O in the gas phase has reached a mature level of understanding. Decomposition of CH_2O to CO + H_2 at high temperatures is dominated by a radical dissociation channel.[2] The initiation step is the molecular fragmentation into H + HCO, which is an endothermic reaction with little energy barrier[3] above the reaction enthalpy (ΔH(298 K) = 88.19 kcal mol^{-1}). The energy barrier of the competing unimolecular decomposition into CO + H_2 has been found to lie in the range of 80−82 kcal mol^{-1} with a reaction enthalpy of ΔH(298 K) = −0.47 kcal mol^{-1}.[3]

Decomposition of CH_2O on clean surfaces of the noble metals under UHV and low-temperature conditions is very slow, and molecular desorption of the adsorbed phase is the dominant reaction path. However, experiments indicate that preadsorbed surface oxygen on silver, copper, and gold surfaces catalyzes the decomposition to CO_2 accompanied by H_2 or H_2O.[4,5] On silver, in particular, temperature-programmed desorption spectra following CH_2O adsorption on an Ag(110) surface that had previously been covered with oxygen showed an H_2 desorption peak at 250 K and a subsequent desorption peak of H_2 and CO_2 at 420 K.[6−8] The low- and high-temperature desorption peaks were inferred to be formed from dioxymethylene (CH_2O_2) and formate (CHO_2) decomposition.[6−8] Analysis of DRIFTS spectra of the catalytic surface after CH_2O decomposition at 493 K also suggested that CH_2O_2 and CHO_2 are intermediates in the process leading to CO_2 and CO formation on Ag powder and supported Ag catalyst.[9] On Ag/MnO_x−CeO_2 catalyst, complete oxidation to CO_2 and H_2O at 373 K has been reported,[10] presumably due to the higher concentration of surface oxygen on silver that is supplied by the supported catalyst.[10]

CHO_2 has been found to be the predominant adsorbed intermediate in CH_2O decomposition on a series of surface oxides.[11] Interpretations of EELS and NEXAFS spectra of CHO_2 on the Ag(110) surface indicate that its adsorption takes place on the rows of the surface plane through both oxygen atoms with the OCO plane perpendicular to the surface.[12−14] This adsorption configuration has also been predicted using DFT modeling studies on Cu(111) catalyst.[15] A stable form of formaldehyde intermediate below 225 K on oxidized Ag(110)[7] has been used to characterize important modes of vibration of CH_2O_2. The vibrational modes indicate that CH_2O_2 is adsorbed on the troughs of the Ag(110) surface.[6] A similar adsorption configuration has been predicted using periodic GGA-DFT analysis on Cu(111).[16] Rapid conversion of surface CHO on silver has precluded a detailed experimental examination of its properties. However, modeling using an embedded cluster method shows that CHO is adsorbed on the Ag(111) surface in a weakly bound state.[17] This is in contrast with a considerable adsorption energy of CHO on Cu(111) surface using periodic DFT methods, where the binding energy is calculated to be 30.4 kcal mol^{-1}.[18]

The decomposition of CHO_2 has been found to be one of the rate-limiting steps during methanol oxydehydrogenation on Ag(110).[19] Therefore, a fundamental understanding of methanol and formaldehyde behavior over silver requires a detailed analysis of the stability, site selectivity, and energy profiles of the elementary reactions of CH_2O decomposition on clean and oxidized surfaces. From our ongoing modeling study of the chemistry of methanol (CH_3OH) reaction over silver (Ag(111)),[20] we report here on the decomposition of formaldehyde (CH_2O) in the absence and in the presence of on-surface adsorbed oxygen. In particular, we reveal the site selectivity and stability of CH_2O_2, CHO_2, CHO, CO, and CO_2 intermediates at different surface coverages, the minimum energy paths (MEPs) for decomposition on clean and oxygen-dosed surface, and kinetic parameters of surface reactions.

Computational Technique

DFT-GGA molecular modeling simulations were performed using the plane-wave code Dacapo[21,22] with Vanderbilt ultrasoft

* To whom correspondence should be addressed. E-mail: a.montoya@usyd.edu.au.

10.1021/jp901134d CCC: $40.75
Published on Web 06/19/2009

TABLE 1: Geometrical Parameters, in angstroms and degrees, Frequencies of Vibration (v), in inverse centimeters, Zero-Point Energy (ZPE), in kilocalories per mole, and Atomization Energy (AE), in kilocalories per mole, of Gas-Phase Molecules

					literature[32−34]	
	DFT GGA-PW91 geometry parameters	v (cm^{-1})	ZPE	AE	ZPE	AE
CH_2O	r(CH) = 1.11, r(CO) = 1.22, >CHO = 122, >HCH = 116	2912, 2864, 1824, 1484, 1213, 1153	16.4	358.0	16.1	357.3
CH_2O_2	r(CH) = 1.10, r(CO) = 1.40, >HCH = 117, >OCO = 66	3121, 3023, 1471, 1284, 1197, 1110, 895, 797, 971	19.8	397.0	20.4	404.3
CHO_2	r(CH) = 1.16, r(CO) = 1.24, >OCO = 144, >HCO = 108	2391, 1756, 1218, 826, 749, 647	10.8	386.4	9.6	369.0
CHO	r(CH) = 1.13, r(CO) = 1.20, >HCO = 124	2673, 1943, 1051	8.1	274.7	7.7	270.8
CO	r(CO) = 1.16	2221	3.2	248.9	3.1	256.2
CO_2	r(CO) = 1.18	2487, 1363, 632, 636	7.3	387.0	7.2	381.9

pseudopotentials.[23] The Perdew and Wang nonlocal corrections to the exchange-correlation energy were included self-consistently.[24] The Kohn−Sham equations[25] were solved using a plane-wave basis set of kinetic energy 340 eV, whereas 400 eV was used as a cutoff for the density grid. In test calculations, for higher kinetic energy values, a density cutoff equal to the kinetic energy was used. A Monkhorst−Pack mesh[26] of (6 × 6 × 1) k points was used for the (2 × 2) unit cell, and (4 × 4 × 1) k points were used for the (3 × 3) unit cell.

The Ag surface is represented by periodic slabs with five layers repeated in a supercell geometry with 15 Å of vacuum between them. The three lower layers are maintained at DFT-bulk geometry, and the two upper Ag atom layers are allowed to fully relax. The adsorbate is chemisorbed and fully relaxed on the upper layer of the Ag slab, and the induced dipole moment is taken into account by applying a dipole correction.[27] Analysis of surface coverage dependence has been performed using the (2 × 2) and (3 × 3) unit cells corresponding to 0.25 and 0.11 ML coverage, respectively. The optimization was concluded when the root-mean-square force on the atomic nuclei was less than 0.05 eV/Å. The self-consistent field was affected using an electronic temperature of $k_BT = 0.1$ and 0.0001 eV for the Fermi distribution of the slabs and gas-phase molecules, respectively, with Pulay mixing of the resulting electronic density. Total energies have been extrapolated to $k_BT = 0$ eV. Test calculations on the binding energy at 0.25 ML coverage show that the predicted binding energy is converged within 0.6 kcal mol^{-1}.

The minimum energy paths (MEPs) on the potential energy surface for CH bond scission are calculated using the nudged elastic band (NEB) method[28,29] on the (2 × 2) unit cell. The stable end points of the NEB calculations are allowed to relax to their respective local minima. These end points are connected through a set of at least six images on the elastic band. The images are subsequently allowed to relax using a quasi-Newton algorithm until the forces and energy converge to the MEP connecting the two end points. The MEP search yields a configuration close to the transition state of the reaction, which is further optimized to minimize the forces, leading to identification of the equilibrium position of the transition state.[30] The energy values of the MEP are calculated relative to the energy of reactant species at infinite separations, that is, where the surface species of the initial state are chemisorbed on their most stable adsorption sites in separated unit cells.

The binding energy (E_b) of species on the surface is calculated as the energy difference in their equilibrium configurations between the gas−silver system (E_{g-s}) and the sum of the bare silver slab (E_s) and isolated gas-phase species (E_g), $E_b = E_{g-s} - (E_s + E_g)$. By definition, a positive binding energy indicates an exothermic adsorption. The total energies of isolated gas phase species are calculated in a cubic cell of side length 12 Å with spin polarization corrections. The energy of gas-phase species is converged to <0.7 kcal mol^{-1} with respect to the plane-wave kinetic energy.

Harmonic vibrational frequencies of local minima and saddle points are calculated for all species in their equilibrium configuration by diagonalizing the Hessian matrix, which is approximated via finite differences of forces, determined by displacing each center of the adsorbate by ±0.05 Å along each of the Cartesian coordinates. Silver atoms are frozen during the frequency calculation of surface species.

The calculated geometry and vibrational frequencies of the gas-phase molecules CH_2O, CH_2O_2, CHO_2, CHO, CO, and CO_2 are shown in Table 1. CHO_2 has two nearly degenerate electronic states, $^2B_2$ and $^1A_1$, with $^1A_1$ being slightly more stable.[31] We have adopted the $^1A_1$ electronic state as our reference for calculation of the binding energy of CHO_2. Earlier work has shown that the nature of the $^1A_1$ electronic state is sensitive to the quantum chemistry method used.[32] In our case, normal-mode vibrational analysis shows that $^1A_1$ is a local minimum; that is, all vibrational frequencies are real, as shown in Table 1.

We confirmed the accuracy of our geometries by comparing the zero-point energies (ZPEs) of gas-phase species, calculated from our geometry parameters and vibrational frequencies, with experimental and high-level ab initio calculated values,[32−34] as shown in Table 1, where the deviations are at most 1.2 kcal mol^{-1}. On the other hand, our predicted atomization energies significantly diverge from published values; as expected, high-level ab initio methods are needed for accurate determination of the energy of gas-phase species. This is particularly so for CHO_2 for which high-level electron correlation treatment is required.[32] In the present work, we are interested in relative changes, and the conclusions and trends will not be affected by the prediction of the atomization energy; nevertheless, we must clearly be careful in drawing any conclusions that may be affected by the absolute values of the energy of species in the gas phase.

Stability and Structure of Surface Species. We determine the site selectivity and binding energy of surface species that are involved in the decomposition of CH_2O on the topmost layer of clean and oxidized Ag(111) surface. In previous studies,[20,35,36] we provided adsorption properties for hydrogen, hydroxyl, oxygen, water, and formaldehyde on Ag(111). We focus here on the adsorption of CHO, CHO_2, CH_2O_2, CO, and CO_2 surface species, determining the site selectivity and adsorption geometry on different sites above the topmost layer of Ag(111) at 0.25 ML. The binding energy at 0.11 and 0.25 ML and frequencies of vibrations at 0.25 ML on the most stable adsorption site are compiled in Table 2, and selected geometrical parameters are given in Figure 1.

Formyl (CHO). We found two stable configurations of CHO on Ag(111), each binding via the carbon atom, η_1-(C), with a V-shaped HCO bond angle. The most stable configuration binds

TABLE 2: Binding Energy (BE), in kilocalories per mole, Work Function Change (ΔΦ), in electronvolts, and Vibrational Frequencies (υ), in inverse centimeters, of Surface Species on Ag(111)

	BE		ΔΦ	υ	
	0.11	0.25	0.25	0.25	ZPE
CHO_{bridge}	21.2	22.0	0.11	2803, 1761, 1190, 382, 610, 191, 86	10.0
$CH_2O_{2\text{-bridge}}$	63.5	61.8	0.79	2944, 2912, 1426, 1229, 1158, 1039, 976, 879, 566, 143, 284, 266, 220	20.2
$CHO_{2\text{-bridge}}$	56.1	55.2	0.52	979, 1314, 1589, 2953, 727, 260, 270, 256, 88	13.9
$CO_{2\text{-bridge}}$	1.2	1.1	−0.1	2487, 1363, 632, 636	7.3
CO_{top}	5.5	5.5	−0.1	2221	3.2

to the HCO molecular plane parallel to a bridge, with the carbon atom closer to the surface above an atop site, as shown in Figure 1. CHO also binds C-down to Ag(111), with the carbon atom above a bridge site and the HCO molecular plane perpendicular to the bridge axis. This adsorbed configuration is, however, 1.7 kcal mol^{-1} less stable than adsorption above the bridge site. The energy barrier for CHO diffusion through the bridge sites is 1.9 kcal mol^{-1}. Because the stability of CHO is almost degenerate with a small energy barrier for diffusion, the translation in the HCO molecular plane is energetically facile. Similar degenerate adsorption energies have been predicted using periodic GGA-DFT functionals for different adsorption configurations of CHO on Cu(111) and Pd(111).[37,38]

The binding energy of CHO adsorbed along the bridge site is 21.2 and 22.0 kcal mol^{-1} at 0.11 and 0.25 ML, respectively, revealing only a small molecular CHO interaction energy at low coverage. Experimental determination of the binding energy of CHO on silver is not available to us; however, our predicted binding energy is slightly smaller than that predicted on Cu(111)[37,38] using periodic GGA-DFT methods. The work function change of the Ag(111) surface after CHO adsorption along the bridge site at 0.25 ML is +0.11 eV (2.5 kcal mol^{-1}), and the dipole moment is −0.1 D. These small changes indicate that the magnitudes of electron donation and back-donation effects are nearly the same. The DFT stretching modes are $\upsilon(CH) = 2803\ cm^{-1}$, $\upsilon(CO) = 1761\ cm^{-1}$, $\upsilon(CH) = 1190\ cm^{-1}$, $\upsilon(Ag-O) = 382\ cm^{-1}$, and $\upsilon_{rotation} = 610$, 191, and 86 cm^{-1}. As a result, the ZPE of the adsorbed CHO phase increases by 1.9 kcal mol^{-1} in comparison with the predicted ZPE of CHO in the gas phase. (See Tables 1 and 2.) In particular, the change in ZPE comes from a slight increase in the CH vibrational frequencies and a small contribution from the frustrated translational and rotational vibrations.

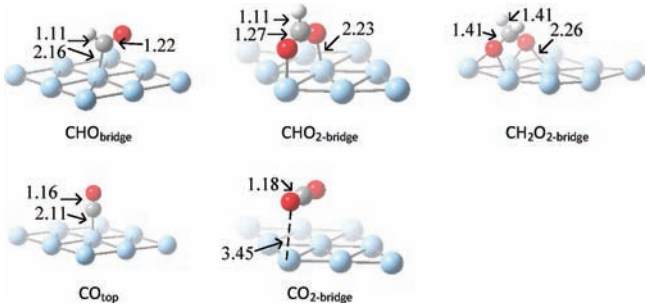

Figure 1. Calculated DFT molecular geometries of adsorbed CHO, CH_2O_2, CHO_2, CO, and CO_2 on a (2 × 2) unit cell of Ag(111). Selected bond lengths in angstroms are depicted. Ag atoms in blue, C atoms in gray, O atoms in red, and H atoms in white.

Formate (CHO_2). We found that the most favorable adsorption configuration of formate on Ag(111) is bidentate bonding to either end of a bridge site, $CHO_{2\text{-bridge}}$, as shown in Figure 1. The carbon atom is centered on the bridge site with the C−O bonds symmetrically oriented toward adjacent atop sites. The O−CH−O molecular plane is perpendicular to the topmost Ag layer and parallel to the axis of the bridge site. Two other less-stable adsorption configurations of the bidentate adsorbed phase, $CHO_{2\text{-hollow}}$ and $CHO_{2\text{-longbridge}}$, are also possible. Each of these has the O−CH−O molecular plane perpendicular to the topmost layer and to the axis of a bridge site. $CHO_{2\text{-hollow}}$ is adsorbed with the carbon atom in the center of a hollow site and the C−O bonds oriented toward a bridge and atop site. $HCO_{2\text{-longbridge}}$ is adsorbed with the carbon atom above the center of a bridge site with the C−O bonds oriented toward opposite hollow sites. The forms $CHO_{2\text{-hollow}}$ and $CHO_{2\text{-longbridge}}$ are 0.2 and 5.8 kcal mol^{-1} less stable than $CHO_{2\text{-bridge}}$ at 0.25 ML coverage.

The binding energy of $CHO_{2\text{-bridge}}$ is 56.1 and 55.2 kcal mol^{-1} at 0.11 and 0.25 ML, respectively, showing a small coverage dependence on the binding energy below 0.25 ML. The work function of the adsorbed phase at 0.25 ML increases by 0.52 eV (12.0 kcal mol^{-1}) compared with the clean Ag(111) surface, and the dipole moment is −0.46 D, implying an electron transfer from the surface toward the adsorbed phase. The DFT stretching modes are predicted to be $\pi(CH) = 979\ cm^{-1}$, $\upsilon(COO) = 1314\ cm^{-1}$, $\upsilon(COO) = 1589\ cm^{-1}$, $\upsilon(CH) = 2953\ cm^{-1}$, $\delta(OCO) = 727\ cm^{-1}$, $\upsilon(Ag-O) = 260\ cm^{-1}$, and $\upsilon_{rotation} = 270$, 256, 88 cm^{-1}, all of which are within 80 cm^{-1} of the observed HREELS modes of formate phases on Ag(110) at 300 K.[13]

Analysis of HREELS spectra shows that formate binds in a monodentate configuration (one of the two oxygen atoms is bound to the surface) at low temperature on Ag(110) and converts to a bidentate configuration (both oxygen atoms are bound to the surface) in an irreversible process upon heating the adsorbed phase to 300 K.[13,39] The bidentate orientation of formate has also been suggested to be the most stable adsorption configuration on Cu(111)[40] and Pd(111).[41]

Previous DFT cluster modeling calculations of formate on Cu(111)[15] show that the monodentate configuration ($CHO_{2\text{-mono}}$) is bound to the surface through one oxygen atom above a hollow site and the other oxygen pointing way from the surface with the O−C−O bond angle pointing toward the adjacent hollow site. We found that on Ag(111), the monodentate configuration is unstable as it moves spontaneously to the bidentate form over different sites of the Ag(111) surface. A restricted optimization shows that $CHO_{2\text{-mono}}$ is 9.9 kcal mol^{-1} less stable than $CHO_{2\text{-bridge}}$. The clear implication is that transformation of the bidentate to the monodentate configuration of formate is activated and therefore cannot easily take place at low temperature.

Dioxymethylene (CH_2O_2). The most stable configuration of CH_2O_2 adsorbs on Ag(111) with the carbon atom over a bridge site and the two C−O bonds oriented toward hollow sites such that the HCH axis is perpendicular to the OCO axis, as shown in Figure 1. A similar stable configuration of CH_2O_2 has been proposed on Cu(111).[16] CH_2O_2 also adsorbs with the O−C−O plane parallel to a bridge site and the C−H bonds directed toward the hollow sites. This adsorbed configuration is, however, 14.7 kcal mol^{-1} less stable.

The binding energy of the most stable configuration of CH_2O_2 on Ag(111) is 63.5 and 61.8 kcal mol^{-1} at 0.11 and 0.25 ML, respectively, showing a small repulsive interaction at low coverage. The work function at 0.25 ML increases by 0.79 eV (18.2 kcal mol^{-1}), and the dipole moment is −0.63 D, implying an ionic nature of the adsorbed phase. The DFT stretching modes

are predicted to be $\upsilon(OCO) = 566\ cm^{-1}$, $\upsilon(OCO) = 879\ cm^{-1}$, $\upsilon(OCO) = 976\ cm^{-1}$, $\rho(CH_2) = 1039\ cm^{-1}$, $\tau(CH_2) = 1158\ cm^{-1}$, $\omega(CH_2) = 1229\ cm^{-1}$, $\delta(CH_2) = 1426\ cm^{-1}$, $\upsilon(CH_2) = 2912$ and $2944\ cm^{-1}$, $\upsilon(Ag-O) = 143\ cm^{-1}$, and $\upsilon_{rotational} = 284$, 266, and $220\ cm^{-1}$. The frequency values are within $200\ cm^{-1}$ of those assigned to CH_2O_2 on Ag(110).[6] After adsorption, the ZPE of the adsorbed CH_2O_2 phase increased by 0.2 kcal mol^{-1} in comparison with the predicted ZPE of CH_2O_2 in the gas phase.

Carbon Monoxide (CO). The adsorption of CO has been studied on transition and noble metals by a variety of experimental and theoretical techniques. Previous ab initio DFT modeling on selected close-packed transition and noble metals surfaces shows that current GGA functionals tend to overestimate the adsorption energy of CO for sites with high metal coordination and fail to predict the site preference on Cu, Rh, and Pt.[42] Empirical corrections based on the vibrational C−O stretching mode have been suggested to reduce the binding energy errors for this system.[43] However, the GGA-PW91 functional seems to behave properly in the CO/Ag(111) system. Surface potential measurements on Ag(111) covered by CO molecules indicate that CO is physically adsorbed with an adsorption energy of 6.4 kcal mol^{-1} at low coverage on the atop site.[44] We found the binding energy of CO on the atop sites to be 5.5 kcal mol^{-1} at 0.11 and 0.25 ML coverage, which is in good agreement with the experimental data. Binding energies to the bridge, fcc, and hcp sites are 5.0, 4.8, and 4.6 kcal mol^{-1}, respectively, implying a slight preference for adsorption on the atop sites. We observed no significant energy barrier above the endothermicity of the reaction for CO diffusion from an atop to a bridge site, which implies that CO is mobile on the surface below 0.25 ML coverage. Assuming an energy barrier of 0.5 kcal mol^{-1}, we estimated a frequency of $22\ cm^{-1}$ for the frustrated parallel vibration. The frequency is small enough for the frustrated translation to be treated better as a free translation.

The DFT C−O stretching mode on the atop site is $2134\ cm^{-1}$, consistent with the $2137\ cm^{-1}$ HREELS stretching mode observed after CO adsorption on Ag(111) at low coverage and temperatures below 35 K.[45] The C−O stretching mode in the adsorbed state is similar to the stretching mode of the isolated CO molecule calculated to be $2221\ cm^{-1}$, which is in accordance with the physical nature of CO adsorption on Ag(111). Correction for ZPE decreases the binding energy by 0.9 kcal mol^{-1}. The small decrease comes from the conversion of the perpendicular translation and rotations of adsorbed CO into vibrations. The weak interaction is also manifested in small changes in the work function after CO adsorption. The work function decreases by 0.1 eV (2.3 kcal mol^{-1}) after adsorption on the atop site, whereas the work function increases by 0.45 (10.4 kcal mol^{-1}), 0.6 (13.8 kcal mol^{-1}), and 0.85 eV (19.6 kcal mol^{-1}) after adsorption on the bridge, fcc, and hcp sites. Relative changes in the work function can be related to the site preference for CO adsorption. The increase in the work function after CO adsorption on the bridge, fcc, and hcp sites indicates a small net flow of electrons from the surface to the antibonding states of CO causing a slight decrease in the stability on the surface.

Carbon Dioxide (CO_2). In the present work, we observe no site selectivity of CO_2 on Ag(111). The binding energy at the bridge site, as shown in Figure 1, is 1.2 kcal mol^{-1} at 0.11 and 0.25 ML, indicating a very weak interaction with the surface. The binding energy is unchanged when the CO_2 molecule moves to other adsorption sites, mainly because the CO_2 molecules binds in a flat configuration far from the topmost layer. The adsorbed CO_2 therefore retains the translational degrees of freedom parallel to the surface plane.

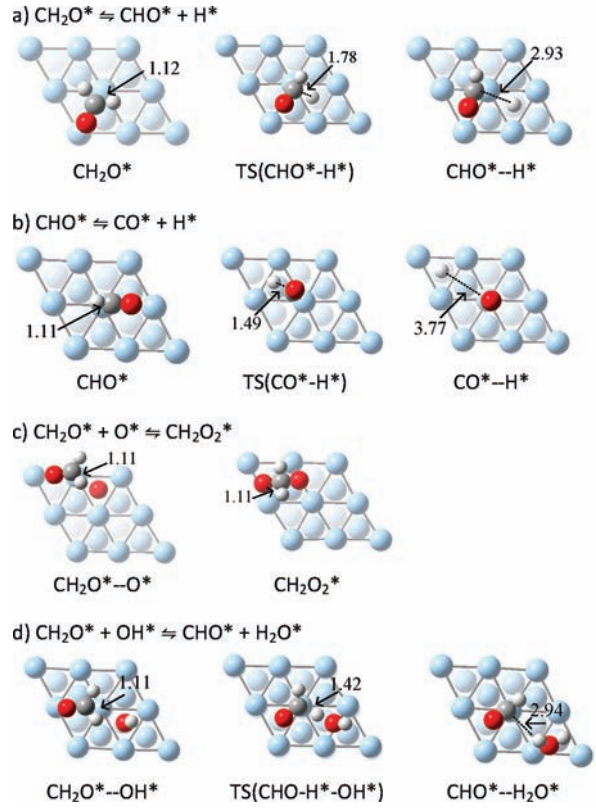

Figure 2. Top view of the calculated DFT molecular geometries CH_2O decomposition on clean and oxygen- and hydroxyl-covered Ag(111). C−H bond length in angstroms is depicted. Ag atoms in blue, C atoms in gray, O atoms in red, and H atoms in white.

The work function decreases by 0.1 eV (2.3 kcal mol^{-1}) after adsorption of CO_2. This small value indicates a small net flow of electrons, mainly because of the physical nature of the adsorption configuration. The GGA-PW91 vibrational bending mode is shifted $121\ cm^{-1}$ to lower values, whereas the symmetric and asymmetric stretching modes are almost unchanged compared with the predicted values of isolated CO_2. Changes in the frequency values after adsorption make very little change to the ZPE corrections to the binding energy. Therefore, the enthalpy of the adsorbed phase approaches the enthalpy in the gas phase. DFT binding energy and vibrational frequencies are consistent with experimental observations. The vibrational energies of the fundamental modes of adsorbed CO_2 on Ag(111) at 40 K agree with the gas-phase values within the accuracy of the measurements,[46] confirming that CO_2 adsorbs weakly on silver. However, adsorption of CO_2 can be promoted by preadsorbed oxygen because of the formation of carbonate species, as has been observed on Ag(100) surfaces.[47]

Minimum Energy Paths of Formaldehyde Decomposition. The DFT-calculated molecular structures arising in CH_2O decomposition on the clean Ag(111) surface and in the presence of oxygen and hydroxyl at 0.25 ML coverage are presented in Figures 2−4, and the corresponding ZPE-corrected energy profile is presented in Figure 5. The energies of the various intermediate species are shown in the coadsorbed configuration (*--*) and at infinite separation (* + *), that is, calculating the energy of each adsorbate in separate unit cells in their most stable positions. A summary of the heats of reaction and the activation energies at 0 K of the elementary steps of CH_2O decomposition is given in Table 3.

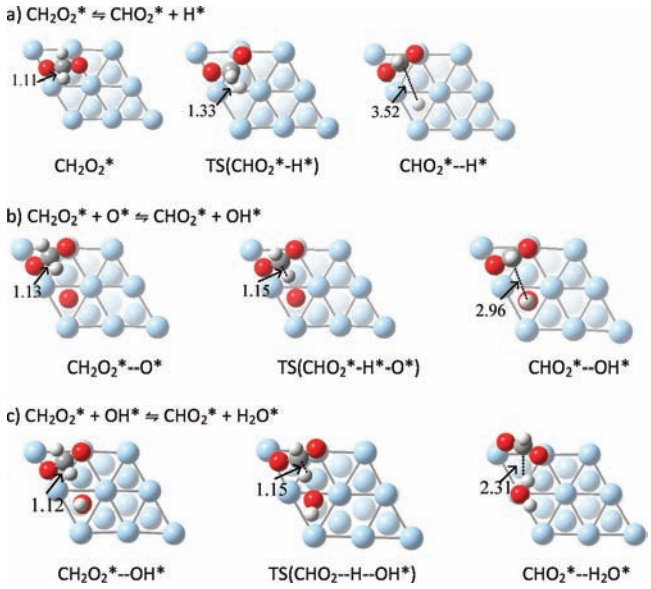

Figure 3. Top view of the calculated DFT molecular geometries of CH_2O_2* decomposition on (a) clean Ag(111), (b) oxygen-covered Ag(111), and (c) hydroxyl-covered Ag(111). C−H bond length in angstroms is depicted. Ag atoms in blue, C atoms in gray, O atoms in red, and H atoms in white.

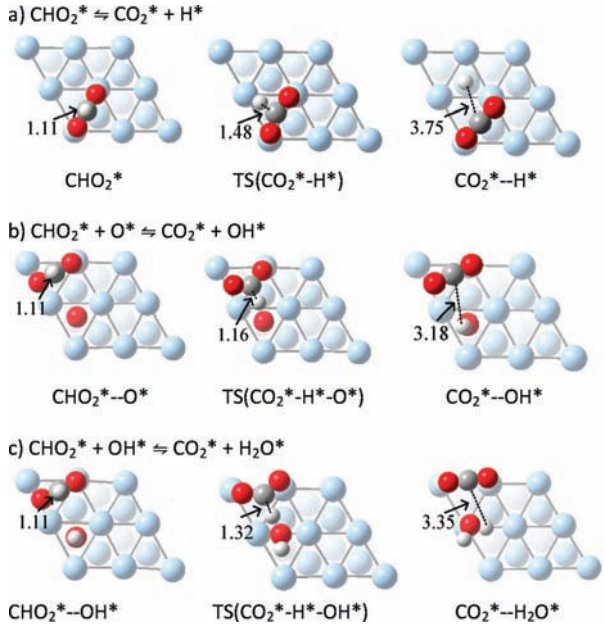

Figure 4. Top view of the calculated DFT molecular structures of CH_2O_2 decomposition on (a) clean Ag(111), (b) oxygen-covered Ag(111), and (c) hydroxyl-covered Ag(111). C−H bond length in angstroms is depicted. Ag atoms in blue, C atoms in gray, O atoms in red, and H atoms in white.

Reactions of CH_2O*. The proposed sequence of steps of hydrogen transfer from adsorbed CH_2O to the clean Ag(111) surface is depicted in Figure 2a,b. CH_2O* is adsorbed with the molecular plane parallel to the surface plane. The first H transfer takes place by rotating the molecular plane of CH_2O perpendicular to the surface plane. In the transition-state structure TS(CHO*−H*), the HCO part binds above the bridge site with the breaking C−H bond elongated by 59% with respect to the initial state. The final product binds HCO on a bridge site and H above a hollow site. The second H-transfer to the surface occurs when the C−O axis of adsorbed CHO is tilted toward the normal surface plane above an atop site. In the TS(CO*−H*) structure, the CO part binds C-down, and the splitting C−H bond is elongated by 34%, with H moving toward a hollow site.

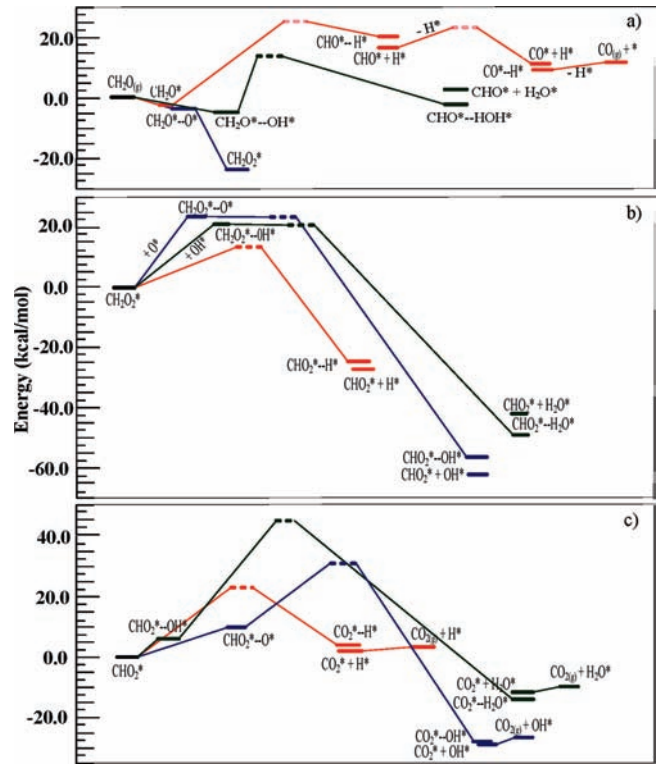

Figure 5. DFT−energy diagram of (a) CH_2O, (b) CH_2O_2, and (c) CHO_2 reactions on clean Ag(111) (red profile), O_{fcc}−Ag(111) (blue profile), and OH_{fcc}−Ag(111) (green profile) surfaces. The energy profile is corrected for the ZPE. Dashed lines correspond to transition estates.

TABLE 3: DFT Enthalpy, $\Delta_r H_{DFT}$(0 K), and Activation Energy ($E_{a\text{-}DFT}$) of Formaldehyde Dehydrogenation and Oxy-Dehydrogenation on Ag(111) Surfaces[a]

	reactions	$\Delta_r H_{DFT}$(0K)	$E_{a\text{-}DFT}$
	Ag(111)/(2 × 2) unit cell	forward	forward
R1	$CH_2O_{(g)} + * \leftrightharpoons CH_2O*$	−2.5	
R2	$CH_2O* + * \leftrightharpoons CHO* + H*$	18.3	28.3
R3	$CHO* + * \leftrightharpoons CO* + H*$	−7.2	7.6
R4	$CO* \leftrightharpoons CO_{(g)}$	4.8	
R5	$CH_2O* + O* \leftrightharpoons CH_2O_2*$	−22.2	
R6	$CH_2O* + OH* \leftrightharpoons CHO* + H_2O*$	5.0	11.8
R7	$CH_2O_2* + * \leftrightharpoons CHO_2* + H*$	−27.9	13.3
R8	$CH_2O_2* + O* \leftrightharpoons CHO_2* + OH*$	−59.8	23.8
R9	$CH_2O_2* + OH* \leftrightharpoons CHO_2* + H_2O*$	−41.2	20.7
R10	$CHO_2* + * \leftrightharpoons CO_2* + H*$	2.6	24.1
R11	$CHO_2* + O* \leftrightharpoons CO_2* + OH*$	−29.3	30.7
R12	$CHO_2* + OH* \leftrightharpoons CO_2* + H_2O*$	−10.7	45.1
R13	$CO_2* \leftrightharpoons CO_{2(g)}$	1.1	

[a] Energy is given in kilocalories per mole.

Dehydrogenation of CH_2O on clean Ag(111) is activated and endothermic overall, as displayed in Figure 5a (red profile). Conversely, the reverse process, which is the multistep H* and CO* recombination to formaldehyde, is an activated exothermic process. Table 3 summarizes the H_2CO dehydrogenation in reactions R1−R4. Formaldehyde dehydrogenation on Ag(111) is thermodynamically and kinetically unfavorable, mainly because the activation energy of the first hydrogen abstraction from adsorbed formaldehyde is much greater than that predicted for the molecular desorption. The energy barrier of CH_2O

decomposition to CHO is, however, 59.9 kcal mol^{-1} lower than the corresponding energy barrier of this reaction in the gas phase, showing the catalytic effect of Ag(111) on the C−H bond scission. Dehydrogenation of CHO to CO is 7.6 kcal mol^{-1} activated and 7.2 kcal mol^{-1} exothermic. Conversely, the reverse step is 14.8 kcal mol^{-1} activated. Therefore, desorption of surface CO to the gas phase ($E_a = 4.8$ kcal mol^{-1}) is kinetically favored over its hydrogenation to HCO.

To investigate the effect of surface oxygen on formaldehyde dehydrogenation on Ag(111), we studied the interaction of formaldehyde with oxygen atoms bound to fcc positions (O_{fcc}) because these are the most stable forms of surface oxygen after exposure of the surface to gaseous oxygen.[48] CH_2O* is slightly stabilized by the presence of O*, as revealed by an increase (0.7 kcal mol^{-1}) in the adsorption energy relative to adsorption on the clean surface. Figure 2c shows that CH_2O reacts with this surface oxygen (reaction R5 in Table 3) to form CH_2O_2. This is an exothermic process ($\Delta H = -22.2$ kcal mol^{-1}) that apparently occurs without any barrier; therefore, the NEB MEP is monotonic from reactant to product, and we therefore do not identify a specific "transition state" for this reaction in either Figure 2c or Figure 5a.

Hydrogen abstraction from CH_2O* by O* was also investigated. However, the initial interaction between the hydrogen and the adsorbed oxygen atom is repulsive. We could find no optimized band for this process as the path adjusts to reaction between the carbon atom from the CH_2O with adsorbed O*, forming CH_2O_2*.

We have also explored the interaction of CH_2O and hydroxyl (OH_{fcc}) on Ag(111). We have used OH species bound to fcc sites where OH binds strongly.[35] The CH_2O*−OH* reaction proceeds via hydrogen abstraction to yield H_2O* and HCO* (reaction R6), as shown in Figure 2d. The transition state shows the CH_2O molecular plane moving toward the bridge site with the forming H_2O* on the top site. Figure 5a (green profile) and Table 3 show that water formation from formaldehyde and OH* is endothermic overall with an energy barrier of 14.5 kcal mol^{-1} from the coadsorbed phase CH_2O*−OH*. The further reaction of HCO* will proceed as described above to form CO* and surface hydrogen, H*.

Reactions of CH_2O_2*. It is apparent that in the presence of surface oxygen the main reaction of adsorbed CH_2O is the facile formation of CH_2O_2*. We therefore consider the further reactions of this species in some detail. CH_2O_2* decomposes to CHO_2* through a surface-assisted hydrogen abstraction process (Figures 3a and 5b). The OCO plane in the transition-state structure TS(CHO_2*−H*) moves toward the bridge axis, bending the $-CH_2$ group and bringing one hydrogen atom closer to the surface. The splitting C−H bond is 1.33 Å, which is 21% longer than the unbroken C−H bond. In a subsequent step, the CHO_2* species undergoes decomposition to (CO_2*−H*). The breaking C−H bond at the transition state TS(CO_2*−H*) is 33% elongated with the CO_2 part moving away and H moving closer to the surface.

The oxydehydrogenation of CH_2O_2* in the presence of O* generates CHO_2* and OH*. The reaction is initiated by bending the $-CH_2$ group and slightly elongating the breaking C−H bond, as shown in TS(CHO_2*−H*−O*) (Figure 3b). In contrast, CH_2O_2* reaction with OH* generates CHO_2* and H_2O*, as shown in Figure 3c. In this case, the TS(CHO_2*−H*−OH*) is characterized by the CHO_2* part moving along the bridge site and the nascent H_2O* part moving toward an atop site.

Figure 5b and reactions R7−R9 in Table 3 present the energetics of these elementary reactions of CH_2O_2*. The decomposition is exothermic by 27.9 kcal mol^{-1}. However, there is a barrier of 13.3 kcal mol^{-1}, which is clearly lower than that for the first hydrogen abstraction from CH_2O* on the clean surface. Reaction of CH_2O_2* with O* to yield CHO_2* + OH* is strongly exothermic (59.8 kcal mol^{-1}), with an activation energy of 23.8 kcal mol^{-1}. The energy barrier is a result primarily of the CH_2O_2* interaction with O* in the coadsorbed phase CH_2O_2*−O*. (See Figure 5b.) Reaction of CH_2O_2* with OH* follows a similar energy path, with the repulsive interaction in the coadsorbed phase of CH_2O_2*−OH* accounting for essentially all of the 20.7 kcal mol^{-1} energy barrier to product formation.

The removal of CH_2O_2* is thus always activated, which accounts for the detection of CH_2O_2* as an intermediate in the reaction. The lowest barrier in the (2 × 2) cell is for the decomposition on the clean surface (13.4 kcal mol^{-1}). There are strong repulsive interactions between CH_2O_2* and either O* (24.7 kcal mol^{-1}) or OH* (20.7 kcal mol^{-1}). However, it should be noted that the repulsive interaction energy between CH_2O_2* and O* decreases to 6.0 kcal mol^{-1} in a (3 × 3) unit cell and that oxygen-assisted CH_2O_2* decomposition is not so energetically unfavorable at low O* coverage; the overall activation energy and its coverage dependence will be determined by the relative magnitudes of the frequency factors for the direct and oxygen-assisted rate constants. The observed[10] enhancement of formaldehyde decomposition on oxygen-rich supported silver catalyst silver probably derives more from the influence of O* on the formation of CH_2O_2* than on the subsequent reactions of this species.

Reactions of CHO_2*. As for CH_2O_2*, subsequent reactions of CHO_2* studied here all lead to dehydrogenation, in this case to yield CO_2, with the fate of the hydrogen depending on the reactant. In the surface decomposition of CHO_2* to form CO_2*−H* (Figure 4a), the breaking C−H bond at the transition state TS(CO_2*−H*) is 33% elongated with the CO_2 part moving away and H moving closer to the surface. Oxydehydrogenation of CHO_2* by O* leads to CO_2* and OH*, as shown in Figure 4b. The CHO_2 molecular plane moves toward the surface, bringing one hydrogen atom closer to the O* species. The TS(CO_2*−H*−O*) is characterized by placing the CO_2* part along the bridge site and the OH* part on the three hollow site. The splitting C−H bond in the TS(CO_2*−H*−O*) is 1.160 Å, and the forming O−H bond is 1.82 Å long. Reaction of CHO_2* with OH* produces CO_2* and H_2O* as final products of reaction (Figure 4c). The −CH group moves toward the OH* and brings the CO_2* group over the bridge and the nascent H_2O* part toward an atop site.

The energy paths of these reactions of CHO_2* are presented in Figure 5c, and Table 3 (reactions R10−R12) summarizes the heat of reaction and activation energies. Surface-assisted CHO_2* decomposition to CO_2* + H* is 2.6 kcal mol^{-1} endothermic with an activation energy of 24.1 kcal mol^{-1}. Reactions with O* or OH* are exothermic (29.3 and 10.7 kcal mol^{-1}, respectively) but with substantial activation barriers (30.7 and 45.1 kcal mol^{-1}, respectively). The increase in the activation energy with respect to the surface-assisted decomposition partially comes from repulsive interactions of CHO_2* with the oxidant (10.8 and 5.0 kcal mol^{-1}, respectively). The energy release after reaching the transition state is very large (60.2 and 58.7 kcal mol^{-1}, respectively), making the rates of the reverse steps very slow. The repulsive energy between CHO_2* and O* decreases from 10.9 kcal mol^{-1} in the (2 × 2) unit cell to 1.7 kcal mol^{-1} in a (3 × 3) unit cell and suggests that oxydehydrogenation of CHO_2 in the (3 × 3) unit cell might become

competitive with the direct decomposition. Overall, the abstraction of hydrogen from CHO_2* is, therefore, more activated than the hydrogen abstraction from CH_2O_2*, indicating a larger stability of CHO_2* compared with CH_2O_2*.

Fate of Adsorbed Oxides, CO* and CO_2*. We found that dissociation of CO* and CO_2* is kinetically and thermodynamically unfavorable with respect to molecular desorption. In the case of CO_2*, the surface-assisted C−O scission reaction enthalpy is endothermic by 58.6 kcal mol^{-1} (with the adsorbed CO and O at infinite separation above atop and fcc sites, respectively). CO_2 desorption is energetically favorable because the reaction at 0.25 ML is 1.2 kcal mol^{-1} activated. Decomposition of adsorbed CO to surface atomic species is 103.4 kcal mol^{-1} endothermic (with the adsorbed C and O at infinite separation above fcc sites). CO desorption is, therefore, dominant because it is 5.5 kcal mol^{-1} activated at 0.25 ML.

Conclusions

Molecular modeling using periodic density functional theory has identified the intermediates and reaction pathways in the dehydrogenation of formaldehyde on the clean and preoxidized Ag(111) surface. The intermediates CH_2O_2, CHO_2, and CHO are chemisorbed through the bridge sites, whereas CO and CO_2 are weakly adsorbed with no strong preference for a particular surface site on clean Ag(111) slabs. The energy barriers to molecular diffusion are observed to be small, and the species can be expected to translate rapidly on the Ag(111) surface.

Dehydrogenation of formaldehyde occurs through a combination of surface-assisted processes including decomposition and reaction with surface O and surface OH. Dehydrogenation over clean Ag(111) is thermodynamically and kinetically unfavorable because of a large energy barrier for, in particular, the first C−H bond scission. However, on-surface oxygen atoms (O_{fcc}) promote CH_2O decomposition through the barrierless formation of CH_2O_2 surface species; reaction with OH can also form this species but with substantial energy barrier.

Further reaction of CH_2O_2* sees the loss of hydrogen to form CHO_2*. Oxidative processes are inhibited by repulsive interactions with surface O* and OH*, and the decomposition in a (2 × 2) unit cell of CH_2O_2*, therefore, is likely to occur by direct dehydrogenation. Although the repulsive interactions of CHO_2* with O* and OH* are somewhat weaker than those for CH_2O_2*, direct dehydrogenation is again kinetically favored (activation energy 24.1 kcal mol^{-1}). The formation of H_2 as a product under oxidizing conditions appears to occur as a result of the recombination of surface hydrogen atoms, H*, created in the direct decomposition reactions.

Acknowledgment. We acknowledge the Australian National Computational Infrastructure (NCI) for the computational time allocated to this project.

References and Notes

(1) Reuss, G.; Disteldorf, W.; Gamer, A. O.; Hilt, A. Formaldehyde. In *Ullmann's Encyclopedia of Industrial Chemistry*, 6th ed.; VCH: Weinheim, 2001; Vol. A11, p 619.
(2) Irdam, E. A.; Kiefer, J. H.; Harding, L. B.; Wagner, A. F. *Int. J. Chem. Kinet.* **1993**, *25*, 285.
(3) Zhang, X.; Zou, S.; Harding, L. B.; Bowman, J. M. *J. Phys. Chem. A* **2004**, *108*, 8980.
(4) Bowker, M.; Madix, R. J. *Surf. Sci.* **1981**, *102*, 542.
(5) Outka, D. A.; Madix, R. J. *Surf. Sci.* **1987**, *179*, 361.
(6) Stuve, E. M.; Madix, R. J.; Sexton, B. A. *Surf. Sci.* **1982**, *119*, 279.
(7) Wachs, I. E.; Madix, R. J. *Appl. Surf. Sci.* **1980**, *5*, 426.
(8) Barteau, M. A.; Bowker, M.; Madix, R. J. *Surf. Sci.* **1980**, *94*, 303.
(9) Mao, C.-F.; Vannice, M. A. *J. Catal.* **1995**, *154*, 230.
(10) Tang, X.; Chen, J.; Li, Y.; Li, Y.; Xu, Y.; Shen, W. *Chem. Eng. J. (Amsterdam, Neth.)* **2006**, *118*, 119.
(11) Busca, G.; Lamotte, J.; Lavalley, J. C.; Lorenzelli, V. *J. Am. Chem. Soc.* **1987**, *109*, 5197.
(12) Stevens, P. A.; Madix, R. J.; Stohr, J. *Surf. Sci.* **1990**, *230*, 1.
(13) Sexton, B. A.; Madix, R. J. *Surf. Sci.* **1981**, *105*, 177.
(14) Canning, N.; Madix, R. J. *J. Phys. Chem.* **1984**, *88*, 2437.
(15) Gomes, J. R. B.; Gomes, J. A. N. F. *Surf. Sci.* **1999**, *432*, 279.
(16) Morikawa, Y.; Iwata, K.; Terakura, K. *Appl. Surf. Sci.* **2001**, *169*−*170*, 11.
(17) Kokh, D. B.; Buenker, R. J.; Liebermann, H.-P.; Whitten, J. L. *J. Phys. Chem. C* **2007**, *111*, 9914.
(18) Gomes, J. R. B.; Gomes, J. A. N. F. *J. Electroanal. Chem.* **2000**, *483*, 180.
(19) Wachs, I. E.; Madix, R. J. *Surf. Sci.* **1978**, *76*, 531.
(20) Montoya, A.; Haynes, B. S. *J. Phys. Chem. C* **2007**, *111*, 9867.
(21) Hammer, B.; Hansen, L. B.; Nørskov, J. K. *Phys. Rev. B* **1999**, *59*, 7413.
(22) Bahn, S. R.; Jacobsen, K. W. *Comput. Sci. Eng.* **2002**, *4*, 56.
(23) Vanderbilt, D. *Phys. Rev. B* **1990**, *41*, 7892.
(24) Perdew, J. P.; Chevary, J. A.; Vosko, S. H.; Jackson, K. A.; Pederson, M. R.; Singh, D. J. *Phys. Rev. B* **1992**, *46*, 6671.
(25) Hohenberg, P. C.; Kohn, W. *Phys. Rev.* **1964**, *136*, B864.
(26) Monkhorst, H. J.; Pack, J. D. *Phys. Rev. B* **1976**, *13*, 5188.
(27) Neugebauer, J.; Scheffler, M. *Phys. Rev. B* **1992**, *46*, 16067.
(28) Mills, G.; Jonsson, H.; Schenter, G. K. *Surf. Sci.* **1995**, *324*, 305.
(29) Jonsson, H.; Mills, G.; Jacobsen, K. W. *Classical and Quantum Dynamics in Condensed Phase Simulations*; World Scientific: Singapore, 1998.
(30) Culot, P.; Dive, G.; Nguyen, V. H.; Ghuysen, J. M. *Theor. Chimica Acta* **1992**, *82*, 189.
(31) Kim, E. H.; Bradforth, S. E.; Arnold, D. W.; Metz, R. B.; Neumark, D. M. *J. Chem. Phys.* **1995**, *103*, 7801.
(32) Feller, D.; Dixon, D. A.; Francisco, J. S. *J. Phys. Chem. A* **2003**, *107*, 1604.
(33) *NIST-JANAF Thermochemical Tables*, 4th ed.; Chase, M. W., Jr., Ed.; Journal of Physical and Chemical Reference Data, Monograph no. 9, Parts I and II; American Chemical Society and American Institute of Physics for the National Bureau of Standards: Washington, DC, 1998.
(34) Cremer, D.; Kraka, E.; Szalay, P. G. *Chem. Phys. Lett.* **1998**, *292*, 97.
(35) Montoya, A.; Haynes, B. S. *J. Phys. Chem. C* **2007**, *111*, 1333.
(36) Montoya, A.; Schlunke, A.; Haynes, B. S. *J. Phys. Chem. B* **2006**, *110*, 17145.
(37) Greeley, J.; Mavrikakis, M. *J. Catal.* **2002**, *208*, 291.
(38) Lim, K. H.; Chen, Z.-X.; Neyman, K. M.; Roesch, N. *J. Phys. Chem. B* **2006**, *110*, 14890.
(39) Ayre, C. R.; Madix, R. J. *Surf. Sci.* **1994**, *303*, 297.
(40) Sotiropoulos, A.; Milligan, P. K.; Cowie, B. C. C.; Kadodwala, M. *Surf. Sci.* **2000**, *444*, 52.
(41) Zheng, T.; Stacchiola, D.; Saldin, D. K.; James, J.; Sholl, D. S.; Tysoe, W. T. *Surf. Sci.* **2005**, *574*, 166.
(42) Gajdos, M.; Eichler, A.; Hafner, J. *J. Phys.: Condens. Matter* **2004**, *16*, 1141.
(43) Abild-Pedersen, F.; Andersson, M. P. *Surf. Sci.* **2007**, *601*, 1747.
(44) McElhiney, G.; Papp, H.; Pritchard, J. *Surf. Sci.* **1976**, *54*, 617.
(45) Hansen, W.; Bertolo, M.; Jacobi, K. *Surf. Sci.* **1991**, *253*, 1.
(46) Sakurai, M.; Okano, T.; Tuzi, Y. *J. Vac. Sci. Technol., A* **1987**, *5*, 431.
(47) Campbell, J. M.; Reiff, S.; Block, J. H. *Langmuir* **1994**, *10*, 3615.
(48) Li, W.-X.; Stampfl, C.; Scheffler, M. *Phys. Rev. B: Condens. Matter* **2002**, *65*, 075407/1.

JP901134D